

71. Vogel (6) recommended allowing a minimum of 1 pipe diameter downstream of an entrance to a pipe to develop a recognizable approximation to a parabolic velocity profile; because the profile in the entrance is not uniform, distances here would be even greater. For full (99%) development of the profile, the entrance length is equal to $0.116 Re \cdot r$. J. K. B. Krijger *et al.* [*J. Biomech.* **22**, 1193 (1989)] found that velocity profiles did not return to a parabolic velocity distribution for 30 to 80 pipe diameters downstream of a confluence of vessels.
72. L. S. Smith, *J. Morphol.* **113**, 261 (1963).
73. J. Browning, *Zoomorphology Berl.* **96**, 243 (1980).
74. G. B. Bourne, J. R. Redmond, D. D. Jorgensen, *Physiol. Zool.* **63**, 140 (1990).
75. J. Voltzow, *Zoomorphology Berl.* **105**, 395 (1985).
76. B. R. McMahon and L. E. Burnett, *Physiol. Zool.* **63**, 35 (1990).
77. E. H. Gladfelter, *Biol. Bull. Woods Hole, Mass.* **165**, 619 (1983).
78. J. C. Grimmer and N. D. Holland, *Zoomorphology Berl.* **94**, 93 (1979).
79. J. R. Blake, N. Liron, G. K. Aldis, *J. Theor. Biol.* **98**, 127 (1982).
80. W. F. Pickard, *Prog. Biophys. Mol. Biol.* **37**, 181 (1981).
81. F. W. Ewers and J. B. Fisher, *Am. J. Bot.* **76**, 645 (1989).
82. Crustacea (Arthropoda) with dendrobranchiate or trichobranchiate gills [P. A. McLaughlin, in *The Biology of the Crustacea*, vol. 5, *Internal Anatomy and Physiological Regulation*, L. H. Mantel, Ed. (Academic Press, New York, 1983), pp. 1–52] have a distributed transfer region in which a Murray's law system has not evolved. The most common gill type in the decapod crustaceans, the phyllobranchiate gill, shows a typical planar transfer geometry. The exchange surface of dendrobranchiate and trichobranchiate gills is clearly distributed in three-dimensional space, but there is no evidence of division of the channels between the filaments into some hierarchy of branched vessels. This example may be akin to straining at gnats. Such a distributed gill geometry may be the only option for these animals that increases gill surface area over the phyllobranchiate condition and yet is still compatible with molting. On the other hand, here, too, no shear stress signal is available; the epidermal cells on the gills are covered by the cuticle.
83. The problem of how branching is controlled in these diverse systems has yet to be addressed.
84. M. LaBarbera, *J. Exp. Mar. Biol. Ecol.* **55**, 185 (1981).
85. C. B. Jorgensen *et al.*, *Mar. Ecol. Prog. Ser.* **34**, 69 (1986).
86. N. R. Silvester and M. A. Sleigh, *J. Mar. Biol. Assoc. U.K.* **64**, 859 (1984).
87. F. R. Bernard, *Biol. Bull. Woods Hole, Mass.* **146**, 1 (1974).
88. P. R. Walne, *J. Mar. Biol. Assoc. U.K.* **52**, 345 (1972).
89. H. U. Riisgard, *Mar. Ecol. Prog. Ser.* **47**, 129 (1988).
90. H. D. Green, in *Medical Physics*, O. Glasser, Ed. (Year Book, Chicago, 1950), vol. 2, pp. 228–251.
91. A. S. Iberall [*Math. Biosci.* **1**, 375 (1967)] criticized the vessel dimensions presented by Green (90), in particular the values for the aorta and large arteries, and presented alternative values based on averages. As explained above, such averages can hide the pattern to be studied. Some idea of the variation can be gathered from Iberall's figure 2, where the diameters of the largest arteries vary by a factor of 2.
92. W. F. Ganong, *Review of Medical Physiology* (Lange Medical, Los Altos, CA, 1975).
93. H. M. Reisswig, *J. Morphol.* **145**, 493 (1975).
94. A. C. Burton, *Physiology and Biophysics of the Circulation* (Year Book, Chicago, 1972).
95. G. P. Bidder, *Q. J. Microsc. Sci.* **67**, 293 (1923).
96. I thank A. Biewener, P. Davies, and S. Vogel for helpful comments on this manuscript. This work was supported in part by NSF grant BSR 84-06731.

In Situ Interfacial Mass Detection with Piezoelectric Transducers

MICHAEL D. WARD* AND DANIEL A. BUTTRY

The converse piezoelectric effect, in which an electric field applied across a piezoelectric material induces a stress in that material, has spurred many recent developments in mass measurement techniques. These methods commonly rely on the changes in the vibrational resonant frequency of piezoelectric quartz oscillators that result from changes in mass on the surface of the oscillator. The dependence of frequency on mass has been exploited extensively for mass measurements in vacuum or gas phase, for example, thickness monitors for thin-film preparation and sensors

for chemical agents. Advances in piezoelectric methodology in the last decade now allow dynamic measurements of minute mass changes ($<10^{-9}$ grams per square centimeter) at surfaces, thin films, and electrode interfaces in liquid media as well. Mass measurements associated with a diverse collection of interfacial processes can be readily performed, including chemical and biological sensors, reactions catalyzed by enzymes immobilized on surfaces, electron transfer at and ion exchange in thin polymer films, and doping reactions of conducting polymers.

THE SIGNIFICANCE OF INTERFACIAL PROCESSES IN RESEARCH and commercial applications (such as sensors, electroplating, and corrosion) has stimulated the development of methodologies that probe interfacial processes and chemistry at surfaces and thin films. Advances in piezoelectric methods in the last decade now make possible in situ determination of minute mass changes that occur at thin films and surfaces under a variety of conditions, including liquid media. The low cost and procedural and

conceptual simplicity of these methods portend broad development of commercial and research applications. In this article we discuss the fundamental properties, methodology, and examples of recent applications that highlight the versatility of these mass-sensing piezoelectric transducers.

Piezoelectricity

In 1880, Jacques and Pierre Curie discovered that a mechanical stress applied to the surfaces of various crystals, including quartz, rochelle salt ($\text{NaKC}_4\text{H}_4\text{O}_6 \cdot 4\text{H}_2\text{O}$), and tourmaline, afforded a corresponding electrical potential across the crystal whose magnitude was proportional to the applied stress (1). This behavior is referred to as the piezoelectric effect, which is derived from the

M. D. Ward is in the Central Research & Development Department, E. I. duPont de Nemours and Co., Inc., P. O. Box 80328, Wilmington, DE 19880-0328. D. A. Buttry is in the Department of Chemistry, University of Wyoming, Laramie, WY 82071-3838.

*Present address: Department of Chemical Engineering and Materials Science, University of Minnesota, 421 Washington Avenue, S.E., Minneapolis, MN 55455.

Greek word *piezein* meaning to press. The charges generated in the quartz crystal are due to the formation of dipoles that result from the displacement of atoms in an acentric crystalline material. Shortly after their initial discovery, the Curies experimentally verified the converse piezoelectric effect in which application of a voltage across these crystals afforded a corresponding mechanical strain. The "motor generator" properties associated with piezoelectricity were eventually exploited for the development of underwater sound transducers (sonar) and electromechanical devices such as speakers, microphones, and phonograph pickups (2).

In the 1920s, Cady demonstrated that the converse piezoelectric effect could be exploited for the construction of very stable oscillator circuits, wherein application of an alternating electric field across a quartz crystal substrate results in an alternating strain field. This causes a vibrational, or oscillatory, motion in the quartz crystal, resulting in the generation of acoustic standing waves. Depending on various criteria (see below), the quartz oscillator exhibits a strong preference to vibrate at a characteristic resonant frequency. Impedance analyses generally reveal sharp conductance peaks at this frequency, indicative of high quality factors Q , the ratio of energy stored to energy dissipated per cycle; values of Q can exceed 100,000. Because quartz crystals vibrate with minimal energy dissipation, they are nearly ideal oscillators; their low cost, ruggedness, low defect concentration, ready fabrication, and chemical inertness have resulted in their wide use in frequency control and filter circuits (2-4).

The electromechanical coupling and stresses resulting from an applied electric field depend on the crystal symmetry, angle of cut of the crystal substrate, and configuration of the excitation electrodes used to apply the electric field across the crystal. The various modes of electromechanical coupling result in different types of acoustic waves, modes of propagation, and particle displacements, as exemplified by modes of thickness shear, face shear, longitudinal, surface acoustic wave (SAW), and shear horizontal. Generally, crystals are carefully cut and modified, and the dimensions and electrode arrangement carefully controlled, so that unwanted modes can be separated in the spatial and frequency domains from the desired mode. For example, AT-cut quartz is obtained by cutting wafers of quartz at approximately 35° from the z -axis. Application of an alternating field across the thickness of an AT-cut quartz crystal by two excitation electrodes on opposite sides of the crystal results in shear vibration (Fig. 1) in the x -axis direction parallel to the electric field and propagation of a transverse shear wave through the crystal in the thickness direction.

The role of the piezoelectric effect in mass detection is readily explained by example of the thickness-shear mode exhibited by AT-cut quartz crystals. The electric field, and therefore the piezoelectric strain and vibration of the quartz crystal, is essentially confined to the area between the two excitation electrodes. The shear motion that results is directly analogous to transverse waves traveling in a string of length L bound at both ends, where standing waves can result provided their wavelengths are integral divisors of $2L$. A resonant condition with standing waves is satisfied when the string is driven by impulses at a frequency matching the fundamental or one of the harmonic frequencies. The fundamental frequency, f_0 , of the string is $(S/m_g)^{1/2}/2L$, where S is the tension (force) on the string and m_g is the mass per unit length. An increase in m_g results in a decrease in f_0 : consider the thinner strings of a violin compared to those of a bass viol. In the case of the fundamental shear mode of an AT-cut quartz crystal, $f_0 = (\mu/\rho)^{1/2}/2t_q$, where μ and ρ are the shear modulus (2.947×10^{11} dyne cm^{-2}) and density (2.648 g cm^{-3}) of quartz, respectively. Increasing the quartz crystal thickness (t_q) results in an increase in wavelength ($\lambda = 2t_q$) and a decrease in the fundamental frequency, analogous to increasing the length of a

string. Also, if the mass can be increased without a change in the thickness of the crystal, the mass per unit length increases and the fundamental frequency decreases.

In 1957 Sauerbrey provided a description and experimental proof (by way of evaporative metal deposition) of the mass-frequency relation for foreign layers deposited on thickness-shear mode crystals that are still widely used today for determination of mass changes at the surface of shear mode transducers (5). This mass-sensing format is commonly referred to as the quartz crystal microbalance (QCM). The derivation of the mass-frequency relation implicitly relies on the assumption that a deposited foreign material exists entirely at the antinode of the standing wave propagating across the thickness of the quartz crystal, so that the foreign deposit could be treated as an extension of the quartz crystal. Thus, the frequency change is calculated as though it were the result of an increase in the thickness of the quartz crystal

$$\Delta f/f_0 = -\Delta t/t_q \quad (1)$$

Appropriate substitution of the terms on the left side of Eq. 1 afford Eq. 2

$$\Delta f = \frac{-2f_0^2 \Delta m}{A \sqrt{\rho_q \mu_q}} = \frac{-2f^2 \Delta m}{nA \sqrt{\rho_q \mu_q}} \quad (2)$$

where Δf is the measured frequency shift, f_0 the fundamental frequency of the quartz crystal prior to a mass change, Δm the mass change, A the piezoelectrically active area, ρ_q the density of quartz, and μ_q the shear modulus. Therefore, a change in the mass per unit area, or the areal density, results in a corresponding change in frequency. Although Eq. 2 is rigorously valid only for infinitesimally thin films that have acoustic impedances identical to that of quartz, in practice it is valid up to loadings approaching 10% of the crystal mass. For larger loadings, an impedance matching method has been reported that compensates for the different acoustic properties of quartz and the foreign material (6). The Sauerbrey equation assumes a uniform distribution of mass on the entire electroded portion of an AT-cut quartz crystal. This is especially noteworthy since the shear amplitude, and therefore the sensitivity to mass changes, decreases from the center to the electrode edge, as evidenced by gas (3, 5, 7-9) and liquid-phase (10) measurements. Thickness-shear devices also can be operated at higher frequencies corresponding to odd ($n = 3, 5, 7, \dots$) harmonics in order to obtain higher sensitivity (Eq. 2).

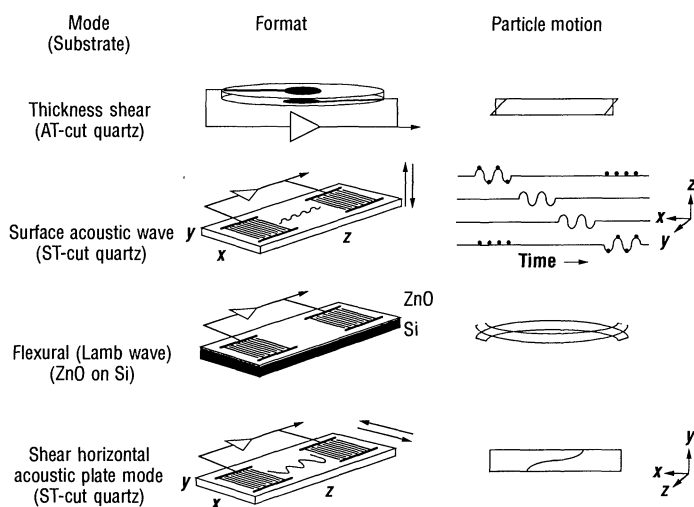


Fig. 1. Representations of typical formats for different piezoelectric devices and their corresponding particle motions. For the SAW and shear horizontal mode, the direction of particle motion is indicated by the arrows.

Table 1. Mass sensitivities of piezoelectric devices; MDM is the minimum detectable mass change at an $S/N = 2$.

Device	Typical f_0 (MHz)	S_m (cm ² g ⁻¹)	MDM (ng cm ⁻²)
SAW (27)	112	151	1.2
SH-APM (9)	104	65	1.0
Lamb (flexure) wave (8, 9)	2.6	951	0.4
QCM (11)	6	14	10

Note that f' , the harmonic frequency, is equal to nf_0 .

Piezoelectric mass detection can also be accomplished with other vibrational modes. Surface acoustic wave (SAW) devices generally comprise two pairs of closely spaced interdigitated electrodes separated by a region of piezoelectric substrate, commonly ST-cut quartz (Fig. 1). An alternating electric field applied by the transmitter pair of electrodes produces periodic strain that launches an acoustic wave. The interaction of the surface wave with a foreign mass in the region between the two arrays results in a change in the SAW velocity and amplitude, which can be sensed by the interaction of the SAW with the interdigitated electrodes at the receiver end as a change in signal intensity produced or a change in the arrival time of the wave with respect to that in a reference SAW device or both. The mechanical properties of the material on the SAW device can influence the correlation between mass and the velocity or amplitude of the SAW (see below). However, if these interferences are negligible, the change in mass of a film in the active region can be determined with Eq. 3, where k_1 and k_2 are material constants of the SAW substrate.

$$\Delta f = (k_1 + k_2)f_0^2 \Delta m/A \quad (3)$$

Recently, acoustic plate wave oscillators that rely on flexure Lamb waves or shear horizontal waves (Fig. 1) have been reported. The flexure mode devices (11, 12) comprise a piezoelectric substrate [for example, zinc oxide (ZnO) on silicon (Si)] that is thin enough so that the flexure mode propagates with minimal energy loss. In contrast to SAW devices, excitation by the interdigitated electrode array induces motion in the entire substrate. The frequency change obtained from a change in mass on the active surface is given by Eq. 4, where ρ and b are the density and thickness, respectively, of the piezoelectric substrate. Shear horizontal-acoustic plate mode (SH-APM) devices use thin quartz plates (about 100 to 200 μm) without an inert support (13). In this case, an alternating field causes particle displacement parallel to the surface and normal to the propagation direction. The mass-frequency relation for the fundamental mode is identical to that of the flexure mode devices (Eq. 4), but operation at higher harmonics conforms to Eq. 5, thereby affording better sensitivity.

$$\Delta f = \Delta m f_0 / 2\rho b A \quad (4)$$

$$\Delta f = \Delta m f_0 / \rho b A \quad (5)$$

Many characteristics of these devices conspire to determine their relative mass sensitivities. For purposes of comparison, mass sensitivity can be couched in the context of operation in an oscillating configuration (see below), so the determination of frequency changes that are consequent to mass changes are of primary interest. Since the mass sensitivities depend on the frequency of operation, common operating frequencies for each device type are given in Table 1. A simplified relation between frequency and mass changes is given by Eq. 6

$$\Delta f/f_0 = -S_m \Delta m \quad (6)$$

where S_m is a proportionality constant with units of square centime-

ters per gram (12). Since the signal-to-noise ratio (S/N) ultimately is the most important criterion in the evaluation of mass sensitivity, the minimum detectable mass change per unit area (MDM) is calculated for $S/N = 2$. When noise and operating frequency are taken into account the mass sensitivities of the devices are similar, with the exception of the QCM shear-mode device. This difference is largely due to the lower operating frequencies of the QCM; operation of the QCM at fundamental frequencies >10 MHz is complicated by the fragility of the very thin plates required. Since the operating frequency of SAW and SH-APM devices is determined by the center-to-center distance between interdigitated electrodes ($f_0 = v/2d$, where v is the acoustic wave velocity and d is the center-to-center distance), their operating frequencies are high compared to shear mode devices. However, mass sensitivity is not the only criterion for choosing a device for a particular application. Ease and appropriateness of use, instrumentation complexity, and cost are also important considerations.

Experimental Considerations

All of these devices can be used for measurements of mass changes in the vapor phase. In fact, considerable effort has been expended on the development of vapor sensors (see below), an area which might be considered a relatively mature subset of the range of applicability of these devices. A key area of interest is the use of piezoelectric devices in liquids, which has been demonstrated for the SH-APM (13), QCM (14–17) and Lamb wave (11) devices. The use of SAW devices in liquid also has been reported (18), although there exists some controversy concerning the actual acoustic mode involved in this application (19). Additionally, operation of SAW devices in liquids can be compromised by compressional dampening of the surface-normal component of the acoustic wave. The influence of the liquid is a less severe problem for shear mode (SH-APM and QCM) devices, since the particle motion is parallel to the surface. However, the vibrational motion of the shear mode transducer surface does induce a standing shear wave in the liquid, which can be

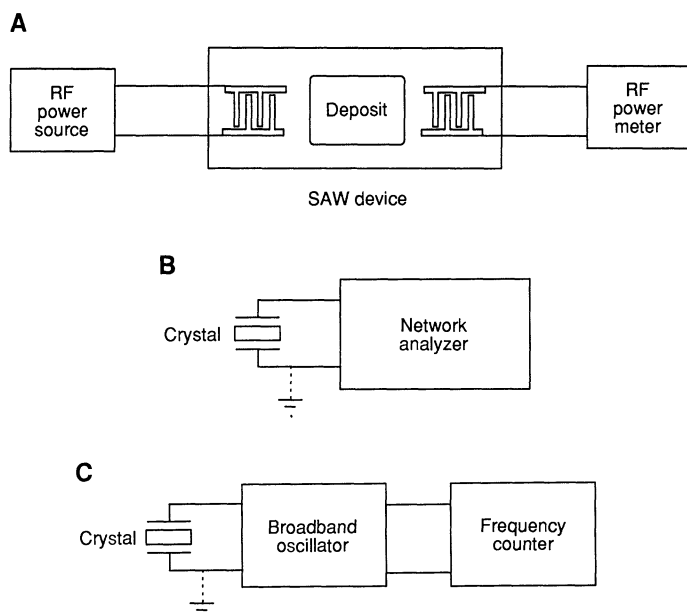


Fig. 2. Schematic diagrams of typical instrumentation for the measurement of different parameters for piezoelectric devices. (A) Amplitude measurement with SAW or SH-APM device, (B) impedance (conductance) measurement with a shear wave device, and (C) resonant frequency measurement with a shear wave device.

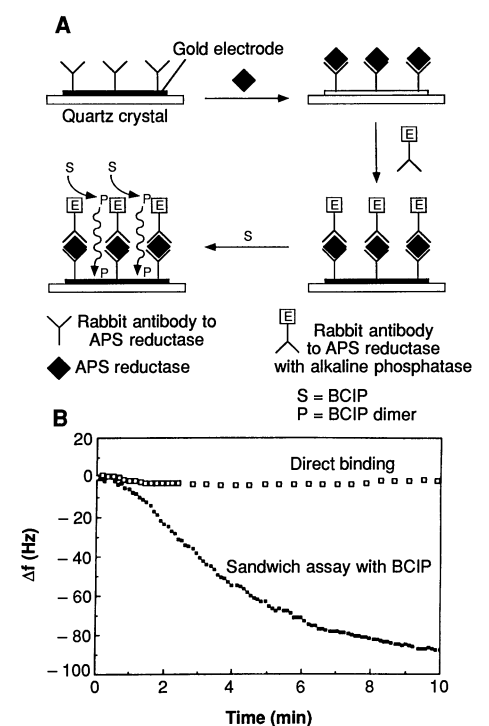
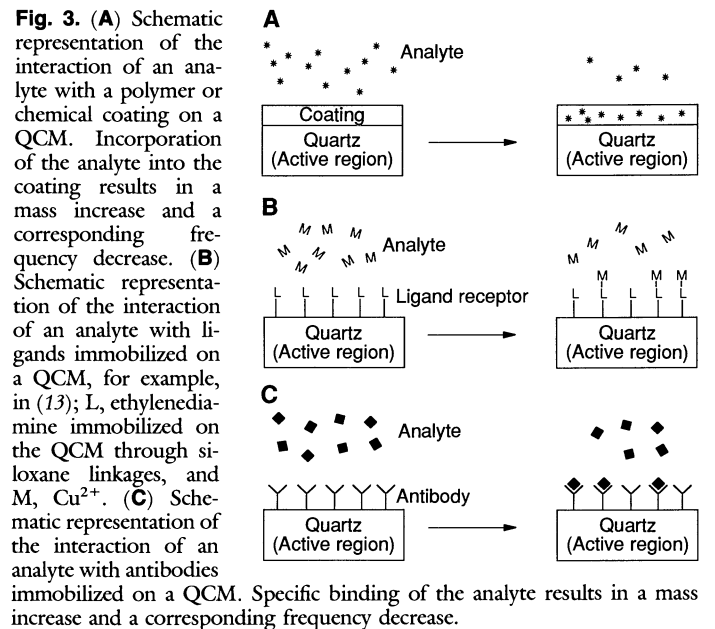
expressed as exponentially damped cosine functions with decay lengths that depend on the frequency and the density and viscosity of the liquid. For a 5-MHz QCM oscillating in pure water at 25°C, this decay length is 250 nm (20), whereas for a 158-MHz SH-APM device it is 50 nm (12, 13). Although the physical properties of the liquid do affect the actual operating frequency, the mass sensitivity is essentially unaffected by the presence of the liquid overlayer. Therefore, the frequency change due to liquid loading for the QCM (20) and the SH-APM (12, 13) can be treated as separable from that due to the mass change at the surface of the device, at least for rigid deposits. There are not yet enough data on the Lamb wave devices for conclusive demonstration of this.

Frequency also depends on the material properties of a foreign material deposited on the transducers. This has been used to considerable advantage in the determination of the viscoelastic properties of polymeric materials of various types with a variety of ultrasonic methods (21), a topic beyond the scope of the present article. For the special case of a thin viscoelastic film, which is most pertinent to the applications described here, an analytical solution of the influence of the film's thickness, density, viscosity, and shear modulus is only available for the QCM (22). This general solution also gives the limiting cases of arbitrarily thick rigid films (that is, perfectly elastic and with zero viscosity) and viscous overlayers (with no elasticity). The former is the Sauerbrey relation and the latter the previously described dependence of the QCM frequency on the density and viscosity of the liquid (20). The dependence on deposit elasticity has also been noted for SH-APM (23) and SAW (24) devices, although quantitative relations are not yet available for these. The measured values of shear modulus and viscosity are frequency dependent, especially for polymeric materials (21), so care in the use of these quantities is required. In addition, at the high frequencies of operation of SH-APM devices, viscous liquids such as glycerol-water mixtures can behave as viscoelastic media. This occurs when the operation frequency is comparable to the intrinsic relaxation frequency of the liquid. The above models can account for this by treating the liquid as Maxwellian with a single relaxation time (22, 23). The possible influence of material properties of the deposit and the liquid on the oscillation frequency of these devices is something that must be closely examined when quantitative mass-frequency relations are sought. The network analysis techniques described below provide a convenient method for determining when this problem exists, as well as sometimes allowing the simultaneous determination of mass and material properties (22).

The type of instrumentation for these devices depends on the nature of the information desired (Fig. 2). Amplitude measurements are made by exciting the transmitting set of interdigitated electrodes with a radio-frequency (RF) power source and detecting the attenuation of the wave amplitude at the receiving set of interdigitated electrodes with an RF power meter. This attenuation most frequently occurs because of mass loading, lossy behavior on the part of the film, or radiation of the energy of the traveling wave into the surrounding medium. It is more common to measure the velocity of the acoustic wave (indirectly) by using the device as a delay line in a resonating element. In this case, the device is connected in the feedback loop of a broadband RF amplifier. This feedback configuration will oscillate at (and therefore track) the resonant frequency of the transducer/thin film composite system, which may be determined with good accuracy (usually to better than 1 part in 10^7) with conventional frequency-counting electronics. The feedback configuration is also the most common for QCM devices and is operationally identical to that used for their use in frequency control applications (2).

A disadvantage of the oscillator method is its inability to unambiguously discriminate between mass and viscoelastically induced

changes that can sometimes result when thin films are present on the transducer surface. However, the use of impedance or network analyzers does allow for this. In this type of experiment, a waveform of alternating polarity and precisely synthesized frequency is applied across the QCM crystal, and the phase and amplitude of the crystal response to this excitation are determined. These are then used to calculate a variety of quantities, including the resonant frequency of the QCM and its Q value. The Q value is a measure of the narrowness of the resonance and the energy dissipation during oscillation and is inversely related to the losses induced from viscous loading by the thin film or a liquid at the QCM surface. Thus, large changes in Q represent a clear signal that the simple, linear mass-frequency relation discussed above is suspect. However, even in such cases it is still possible to calibrate the devices for sensor applications.



One of the strengths of the use of piezoelectric mass sensors is their ability to follow kinetic processes in thin films in real time. The time resolution for detecting mass changes is usually a function of the electronics used for the measurement (see above). The ultimate time resolution is fundamentally limited by the time required for equilibration of the device with a deposited mass. The decay time for this is $Q/\pi f_0$ (25). The AT-cut QCM devices provide a convenient example of this. When used in vapor, the time response is relatively fast because of the large Q values (10^4 to 10^6) for nonviscous loaded devices. However, Q values are small in liquids ($\sim 10^3$) so time resolution is limited to the millisecond range. However, even under these conditions, the kinetics of many types of thin film processes may be monitored in real time, including nucleation, growth, dissolution (26, 27) and electron-transfer reactions at polymer films (17). Measurements of the deposition rates of organometallic complexes on aluminum oxide surfaces, with determination of H-D isotope effects, have also been reported (28).

Piezoelectric Sensors and Biosensors

The advantages of conceptual simplicity, relative ease of modification, chemical inertness of the substrates, ruggedness, low cost, and ready availability of piezoelectric transducers have encouraged the development of various sensor applications. In addition, the sensitivity of piezoelectric transducers is based on the mass per unit area, suggesting miniaturization without losses in sensitivity. The associated electronics are fairly simple and frequency measurements are very precise (<1 part in 10^7). The following examples represent an attempt to illustrate that careful design of interfacial processes can result in viable sensor formats.

Piezoelectric sensors generally have been fabricated by modification of the transducer with a coating that can interact with a desired analyte in a way that the mass of the coating is increased (Fig. 3A). The most common format has involved QCM. Early examples include the detection of hydrocarbons with QCMs coated with chromatographic substrates (29), and commercial instruments for moisture analysis (30) and particle detection (31). Several review articles have appeared that describe various schemes for piezoelectric detection of gas phase analytes using polymer or chemical coatings (32). Detection systems for pollutants, including ammonia, formaldehyde, hydrogen sulfide, ozone, sulfur dioxide, and mercury, have been most extensively investigated. In a similar fashion, SAW (33) and flexural mode (11) devices can be used. The possibility of sensor construction by conventional microfabrication methods may prove advantageous for the eventual commercialization of SAW and flexural devices.

Many of the polymer and chemical coatings used for piezoelectric sensors suffer from poor specificity. As a result, attention has been given to molecular design of active surfaces. Synthetic multilayer coatings have been used for the detection of hydrophobic alcohols, including cholesterol (34), and a cyclodextrin coating exhibited high selectivity for benzene compared to other hydrocarbons (35). Selective detection of hydrocarbons by using zeolite films immobilized on the active region of a SAW device was recently reported (36). Copper (II) has been detected by complexation to ethylenediamine ligands bound by siloxane bonds to the surface of a shear horizontal acoustic plate mode sensor, suggesting applications in trace metals determinations (Fig. 3B) (13). Since the acoustic wave in shear horizontal mode devices propagates through the entire crystal, these sensors may be configured so that the binding layer is on the side opposite the electrodes. This offers the advantage of design simplicity compared to either SAW or flexural mode devices.

A route to analyte detection and identification that circumvents

the need to develop highly specific coatings is pattern recognition, which has been demonstrated for piezoelectric QCM and SAW devices (37). This has allowed for discrimination among different hydrocarbons as well as different alcoholic beverages, with probabilities of correct recognition ranging from 80 to 95%.

Ultimately, the highest specificity may be achieved through immunological interactions between analytes and complementary antibodies immobilized on the piezoelectric transducer. Several research groups have investigated piezoelectric "biosensors" based on the principle of mass increases at the transducer surface that result from specific binding of analytes to immobilized antibodies (Fig. 3C). Detection of the pesticide parathion in the gas phase with a QCM coated with thick films of antibody to parathion was reported (38). Prior to the recognition that piezoelectric transducers could operate while immersed in liquid media, detection of solution analytes commonly involved measurement of the frequency in the dry state, immersion of the crystal/antibody film in a solution containing the analyte of interest, and redetermination of the frequency after removal of the crystal from solution and drying (39). Recently, the detection of nucleic acids by a similar procedure was reported in which polymer-immobilized probe strands on a QCM were incubated with complementary target strands, followed by measurements of the frequency of the dry crystal (40). However, these methods are cumbersome and retention of solvent can cause inaccuracies.

In the last decade, several reports and patents have described direct detection simply by immersing either a QCM or SAW device with immobilized antibody in a solution containing an analyte of interest (18, 41). Most of these investigations have involved the QCM, since energy losses are less severe for shear mode devices than for SAW devices (see above). Although the procedural simplicity of direct detection is attractive, it is questionable whether these devices possess the sensitivity required to detect the small mass changes involved. In the absence of surface modification, such as surface area enhancement, the frequency shifts expected from specific binding of a typical protein to an antibody monolayer are of questionable clinical significance, even if all of the antibody sites are occupied. The frequency response, however, can be amplified by enzymatic reactions with conventional sandwich immunoassay principles. For example, detection of the protein adenosine phosphosulfate (APS)

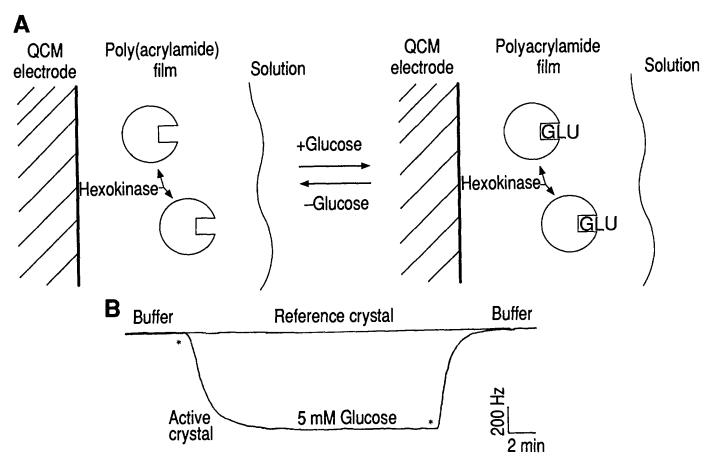
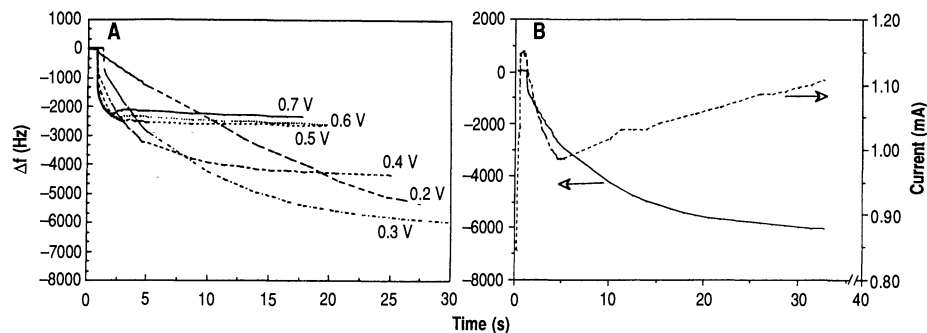


Fig. 5. (A) Representation of the reversible binding of glucose (=GLU) to hexokinase entrapped within a cross-linked polyacrylamide gel. (B) Frequency change of the QCM (reference crystal = polyacrylamide gel without hexokinase; active crystal = gel with hexokinase) upon exposure to 5 mM glucose in pH 7.4 tris buffer. The asterisks indicate the times at which the analyte stream was switched from pure buffer to glucose and buffer, and then back again.

Fig. 6. (A) Frequency response during $\text{TTFBr}_{0.7}$ electrocrystallization at different potentials (as indicated). The faster frequency decrease at early times observed for more positive potentials is indicative of more rapid crystallization under those conditions. At the more positive potentials, however, the frequency decrease ceases at earlier times. (B) Comparison of the current transient and frequency response during $\text{TTFBr}_{0.7}$ electrocrystallization at +0.3 V, 0.1 M $n\text{-Bu}_4\text{N}^+ \text{Br}^-$, and 5×10^{-3} M TTF in acetonitrile. The increasing current signifies that the rate of crystallization is increasing when the mass due to the crystalline deposits is no longer detected by the QCM.



reductase, an enzyme found in sulfate-reducing bacteria, was accomplished with a conjugate of an APS reductase antibody and alkaline phosphatase that is specifically bound, in the presence of APS reductase, to a QCM surface possessing immobilized APS reductase antibody (Fig. 4) (42). Addition of 5-bromo-4-chloroindolylphosphate (BCIP) to the sandwich complex results in enzymatically catalyzed hydrolysis of BCIP to its insoluble dimer, which strongly adheres to the piezoelectrically active area of the QCM surface and results in a decrease in frequency. Whereas direct binding of the APS reductase is not measurable, the enzyme amplification affords sensitivities of $\approx 10^{-11}$ M. A slightly different enzyme amplification approach for immunoassay and nucleic acid detection has been reported recently that involves binding of a homogeneously formed target sandwich complex to avidin immobilized on a QCM surface through a biotinylated conjugate (43).

A somewhat different amplification strategy has been reported for glucose detection (44). Binding of glucose to hexokinase contained in a polyacrylamide polymer film on a QCM afforded frequency changes far in excess of those expected based solely on mass changes (Fig. 5). The large response was attributed to changes in the viscoelastic properties of the polymer upon binding, thus providing analytically useful signals ($S/N \approx 100$) in a convenient one-step format.

Electrochemical Applications of the QCM

Since the first report that the QCM could be used for in situ experiments in conjunction with electrochemical measurements (45), there has been considerable interest in its use to monitor mass changes at electrode surfaces and in thin films on electrodes. When used in this way it is frequently referred to as the electrochemical QCM (EQCM). Several review articles are now available in the area (14, 46). Briefly, the EQCM uses one of the excitation electrodes, which faces the solution, as a working electrode in a conventional electrochemical cell. A significant attribute of the EQCM is its ability to provide correlations between electrochemically induced mass changes at the electrode surface and the charge consumed in the process. Such measurements aid in determination of composition of the deposit, its stoichiometry, and the efficiency of the usage of charge in its deposition. In this section, selected examples of EQCM investigations are described that serve to illustrate the range of issues that can be addressed regarding compositional changes in monolayer and multilayer films induced by electrochemical or chemical processes.

Frequency changes associated with monolayer changes in surface population are not only affected by the mass of the monolayer, but also by mass changes due to solvent or ion content of the monolayer and interactions of the bare surface and adsorbed species with solvent and ions in the electrical double layer. The EQCM has been used to investigate the electrochemically driven formation, onto

metal electrodes, of adsorbed monolayers of oxide (47), halides (48), metal atoms (16, 49), and surfactants whose adsorption characteristics can be altered by redox reactions (50). For example, comparisons of mass and charge revealed that iodide adsorption on gold occurs with complete electron transfer from the adsorbate to the electrode to form essentially zero-valent, adsorbed iodine atoms, whereas for Br adsorption on Au only partial electron transfer occurs (48).

The rates and mechanisms for the electrochemical deposition and dissolution of thick (multilayer) films of a wide variety of materials at electrodes have also been investigated with the EQCM technique. For example, it was recently demonstrated (27) that the mechanism of nucleation and crystal growth of molecular charge transfer salts could be elucidated from the frequency changes at an EQCM during electrocrystallization, a common method for the preparation of these materials. Optimum conditions for crystal growth could be readily determined from comparisons of the mass and charge accumulated during growth of the charge transfer salt $[(\text{C}_6(\text{CH}_3)_6)_2\text{Fe}^{2+}][\text{TCNQF}_4^-]_2$ ($\text{TCNQF}_4 = 2,3,5,6\text{-tetrafluoro-7,7,8,8-tetracyano-}p\text{-quinodimethane}$). Especially revealing were the frequency changes observed for the electrochemical growth of the conducting charge-transfer salt $\text{TTFBr}_{0.7}$ (tetrathiafulvalene) obtained by oxidation of TTF in the presence of $n\text{-Bu}_4\text{N}^+ \text{Br}^-$ (Bu, butyl) in acetonitrile. At low overpotentials (low driving force) the frequency decrease was monotonic for long times, but at more positive potentials the frequency decreased more rapidly at early times, with no further changes at longer times (Fig. 6A). Significantly, the current associated with crystallization was increasing when the frequency was no longer changing (Fig. 6B). The apparent loss of mass sensitivity was attributed to a morphological change in the crystalline deposits, which were no longer rigidly coupled to the QCM because of the onset of dendritic crystallization. The EQCM thus established the optimum conditions for growth of high-quality single crystals by defining the potentials where undesirable dendritic crystallization occurred.

Perhaps the most active area of application of the EQCM to electrochemical problems is its use in the monitoring of compositional changes that accompany redox processes in redox active films and conducting polymers on electrodes. In this context, the EQCM is emerging as a valuable tool in the elucidation of the composition of such systems, the mechanisms of film formation and changes in film composition that occur upon redox cycling. Simultaneous measurement of the mass changes and injection or removal of charge from the film can facilitate understanding of ion and solvent transport in the film. Illustrative of this application is the EQCM investigation of $\text{Cs}_2[\text{NiFe}(\text{CN})_6]$, a nickel derivative of prussian blue, which has been extensively studied by Bocarsly and co-workers (51). These films (ideally) are rigid $\text{NiFe}(\text{CN})_6^{2-}$ lattices with pore sizes (defined by the Fe-C-N-Ni distance along one side of the cubic unit cell) just large enough to accommodate the Cs^+ counterions plus some water molecules. The Fe sites in the lattice structure are

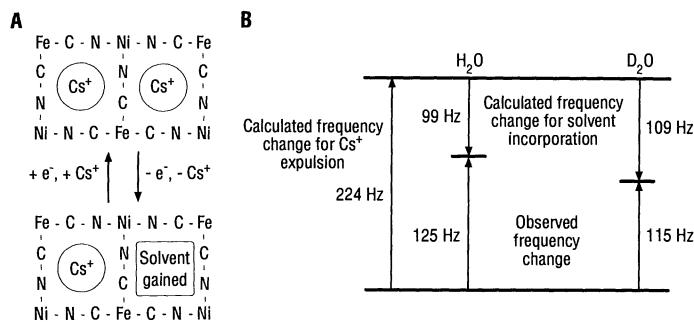


Fig. 7. (A) Representation of the electrochemically induced expulsion of Cs⁺ during oxidation of the Fe sites in the lattice (and vice versa). One-half of the Cs⁺ ions are expelled during the oxidation, and the volume freed by this expulsion becomes available for solvent entrapment within the lattice (indicated) by the box labeled "Solvent gained." (B) Diagram of the frequency changes that occur during the loss of Cs⁺ and gain of solvent during oxidation depicted in (A) for separate experiments in H₂O and D₂O.

redox active, and their oxidation from Fe(II) to Fe(III) causes expulsion of one Cs⁺ per formula unit in order to maintain electroneutrality. A schematic of the transport processes that occur during oxidation is shown in Fig. 7A. The frequency changes, and therefore the mass changes, during this process differ in H₂O and D₂O, indicating the involvement of solvent in the net mass flux during the ion transport process (52). Comparison of the number of expelled Cs⁺ ions required to maintain electroneutrality in this permselective film with the experimentally determined mass change allows determination of the mass change solely due to solvent transport (Fig. 7B). The difference between these values for the H₂O and D₂O experiments is seen to be 10%, consistent with expectations based on the molar masses of these two species (18 and 20 g mol⁻¹, respectively). This example clearly illustrates that mass changes due to ion and solvent transport can be deconvoluted using such isotopic substitution approaches.

The application of acoustic wave devices to monitoring electrochemically induced compositional changes in thin films must be performed with care so as to avoid misinterpretation. As discussed above, the influence of viscoelastic behavior by the thin film can be particularly problematic in regard to the quantitative determination of mass changes from observed frequency changes according to Eq. 2. The use of impedance analysis to determine whether rigid layer behavior prevails for the system at hand is of great benefit in such cases. If a network analyzer is not available it is generally acceptable to vary the thickness of the electroactive film; if the frequency and charge are linearly related, it can be assumed that rigid layer behavior is operative.

Conclusions

The conceptual simplicity of piezoelectric transducers and the commonplace occurrence of mass changes incurred during interfacial processes portends broader applications of this technology in research and commercial applications. The current formats, although suitable for most research applications, are not yet adequate for commercial markets, such as chemical and biological sensors. Further work needs to address issues of sensitivity while maintaining high S/N ratios, as well as new methodologies that exploit the mass sensing properties of these transducers without compromising procedural simplicity. In the case of biosensors, this could best be achieved by methodology that does not require numerous steps that generally accompany immunodiagnostic procedures. Also, methods that do not require direct modification of the transducer with

expensive, and sometimes sensitive, specific receptors is desirable. Ultimately, piezoelectric sensors may use marginally selective coatings coupled with pattern recognition techniques. One significant advantage of piezoelectric sensors is that they sense the mass per unit area. Therefore, sensitivity is not, at least in principle, lost upon miniaturization. Whereas construction of SAW and flexure mode devices is amenable to conventional microfabrication techniques, miniaturization and packaging of QCM devices still requires attention.

Because of their remarkable sensitivity toward mass changes at the submonolayer level, acoustic wave devices of various types will find increasing use in fundamental studies of the solid-liquid interface. However, at this level of sensitivity, consideration must be given to many effects that at present are poorly understood, including interactions of surface charges with ionic species in solution, and density and viscosity changes within the interfacial region. If these devices are to be successfully applied to interfacial studies at the monolayer level (and below), considerable theoretical effort will be required to sort out the influence of such factors on device response and frequency. In addition, other surface spectroscopic methods should be used to aid in their elucidation. Nevertheless, the prospects for fundamental, new knowledge of interfacial behavior from studies using piezoelectric transducers seem promising.

REFERENCES AND NOTES

- P. Curie and J. Curie, *C. R. Acad. Sci.* **91**, 294 (1880).
- W. P. Mason, *Piezoelectric Crystals and Their Application to Ultrasonics* (Van Nostrand, New York, 1950).
- H. Bahadur and R. Parshad, in *Physical Acoustics*, W. P. Mason and R. N. Thurston, Eds. (Academic Press, New York, 1982), pp. 37-171.
- V. E. Bottom, *Introduction to Quartz Crystal Unit Design* (Van Nostrand Reinhold, New York, 1982).
- G. Sauerbrey, *Z. Phys.* **155**, 206 (1959).
- C. S. Lu and O. Lewis, *J. Appl. Phys.* **43**, 4385 (1972).
- K. S. Van Dyke, *Proc. Annu. Freq. Control. Symp.* **10**, 1 (1956); H. Fukuyo, A. Yokoyama, N. Ooura, S. Nonaka, *Bull. Tokyo Inst. Technol.* **72**, 1 (1985).
- I. Koga, *J. Appl. Phys.* **34**, 2357 (1963).
- D. M. Ullevig, J. F. Evans, M. G. Albrecht, *Anal. Chem.* **54**, 2341 (1982).
- M. D. Ward, unpublished results.
- S. W. Wenzel and R. M. White, *IEEE Trans. Electron. Dev.* **35**, 735 (1988).
- _____, *Appl. Phys. Lett.* **54**, 1976 (1989).
- A. J. Ricco, S. J. Martin, T. M. Niemczyk, G. C. Frye, *ACS Symp. Ser.* **403**, 191 (1989).
- D. A. Buttry, in *Electroanalytical Chemistry*, A. J. Bard, Ed. (Dekker, New York, 1990), vol. 17, pp. 1-85.
- P. L. Konash and G. J. Bastiaans, *Anal. Chem.* **52**, 1929 (1980); S. Bruckenstein and M. Shay, *Electrochim. Acta* **30**, 1295 (1985).
- O. Melroy and K. Kanazawa, J. G. Gordon II, D. Buttry, *Langmuir* **2**, 697 (1986).
- M. D. Ward, *J. Phys. Chem.* **92**, 2049 (1988).
- J. E. Roederer and G. J. Bastiaans, *Anal. Chem.* **55**, 2333 (1983).
- G. S. Calabrese, H. Wohltjen, M. K. Roy, *ibid.* **59**, 833 (1987).
- K. K. Kanazawa and J. G. Gordon II, *Anal. Chem.* **57**, 1770 (1985).
- J. D. Ferry, *Viscoelastic Properties of Polymers* (Wiley-Interscience, New York, 1980).
- C. Reed, J. Kaufman, K. K. Kanazawa, *J. Appl. Phys.*, in press.
- G. C. Frye et al., *ACS Symp. Ser.* **403**, 208 (1989).
- D. S. Ballantine, Jr., and H. Wohltjen, *ibid.*, p. 222.
- J. R. Barker, *Mechanical and Electrical Vibrations* (Wiley, New York, 1964).
- R. Schumacher et al., *J. Phys. Chem.* **89**, 4338 (1985); R. Schumacher, A. Muller, W. Stockel, *J. Electroanal. Chem.* **219**, 311 (1987); G. S. Ostrom and D. A. Buttry, *ibid.* **256**, 411 (1988); C. K. Baker and J. R. Reynolds, *ibid.* **251**, 307 (1988).
- M. D. Ward, *J. Electroanal. Chem.* **273**, 79 (1989).
- J. B. Miller and J. Schwartz, personal communication.
- W. H. King, Jr., *Anal. Chem.* **36**, 1735 (1964).
- Moisture Analyzer Model 560.
- M. H. Ho, in *Applications of Piezoelectric Quartz Crystal Microbalances*, C. Lu and A. W. Czanderna, Eds. (Elsevier, New York, 1984), pp. 351-388.
- C. Lu and A. W. Czanderna, in *Microweighing in Vacuum and Controlled Environment*, vol. 4 of *Methods and Phenomena*, A. W. Czanderna and S. P. Wolsky, Eds. (Elsevier, New York, 1984); G. G. Guilbault and J. M. Jordan, *CRC Crit. Rev. Anal. Chem.* **19**, 1 (1988); G. G. Guilbault, *Ion-Selective Electrode Rev.* **2**, 3 (1980); J. J. McCallum, *Analyst* **114**, 1173 (1989).
- H. Wohltjen, *Sensors Actuators* **5**, 307 (1984); _____, D. S. Ballantine, N. L. Jarvis, *ACS Symp. Ser.* **403**, 157 (1989); H. Wohltjen and R. Dessy, *Anal. Chem.* **51**, 1458 (1979); A. Venema, E. Nieuwkoop, M. J. Vellekoop, M. S. Nieuwenhuizen, A. W. Barendsz, *Sensors Actuators* **10**, 47 (1986).
- Y. Okahata, H. Ebato, X. Ye, *J. Chem. Soc. Chem. Commun.* **1988**, 1037 (1988).

35. C. S. Lai *et al.*, *J. Chem. Soc. Perkin Trans. II* **1988**, 319 (1988).
 36. T. Bein, K. Brown, G. C. Frye, C. J. Brinker, *J. Am. Chem. Soc.* **111**, 7640 (1989).
 37. Y. Teki, T. Takui, K. Itoh, *J. Chem. Phys.* **88**, 6134 (1988); D. S. Ballantine, Jr., S. L. Rose, J. W. Grate, H. Wohltjen, *Anal. Chem.* **58**, 3058 (1986); W. P. Carey, K. R. Beebe, B. R. Kowalski, D. L. Illman, T. Hirshfeld, *ibid.*, p. 149; K. Ema, M. Yokoyama, T. Nakamoto, T. Moriizumi, *Sensors Actuators* **18**, 291 (1989).
 38. J. Ngeh-Ngwainbi, P. H. Foley, S. S. Kuan, G. G. Guilbault, *J. Am. Chem. Soc.* **108**, 5444 (1986).
 39. T. K. Rice, U.S. Patent 4,236,893 (1980); *ibid.* 4,314,821 (1982); A. Shons, F. Dorman, J. Najarian, *J. Biomed. Mater. Res.* **6**, 565 (1972).
 40. N. C. Fawcett, J. A. Evans, L.-C. Chein, N. Flowers, *Anal. Lett.* **21**, 1099 (1988).
 41. G. J. Bastiaans, U.S. Patent 4,735,906 (1988); I. Karube, European Patent Application 86307115.5 (1987).
 42. R. C. Ebersole and M. D. Ward, *J. Am. Chem. Soc.* **110**, 8623 (1988).
 43. R. C. Ebersole, J. A. Miller, J. R. Moran, M. D. Ward, *ibid.* **112**, 3239 (1990).
 44. S. J. Lasky and D. A. Buttry, *ACS Symp. Ser.* **403**, 237 (1989).
 45. T. Nomura and M. Iijima, *Anal. Chim. Acta* **131**, 97 (1981).
 46. M. R. Deakin and D. A. Buttry, *Anal. Chem.* **61**, 1147A (1989).
 47. S. Bruckenstein and M. Shay, *J. Electroanal. Chem.* **188**, 131 (1985).
 48. M. R. Deakin, T. T. Li, O. R. Melroy, *ibid.* **243**, 343 (1988).
 49. M. R. Deakin and O. R. Melroy, *ibid.* **239**, 321 (1988); S. Bruckenstein and S. Swathirajan, *Electrochim. Acta* **30**, 851 (1985).
 50. J. J. Donohue and D. A. Buttry, *Langmuir* **5**, 671 (1989).
 51. B. D. Humphrey, S. Simha, A. B. Bocarsly, *J. Phys. Chem.* **91**, 586 (1987).
 52. S. J. Lasky and D. A. Buttry, *J. Am. Chem. Soc.* **110**, 6258 (1988).
 53. Research conducted at the University of Wyoming was supported by the Whitaker Foundation and the Office of Naval Research.

Cell Proliferation in Carcinogenesis

SAMUEL M. COHEN AND LEON B. ELLWEIN

Chemicals that induce cancer at high doses in animal bioassays often fail to fit the traditional characterization of genotoxins. Many of these nongenotoxic compounds (such as sodium saccharin) have in common the property that they increase cell proliferation in the target organ. A biologically based, computerized description of carcinogenesis was used to show that the increase in cell proliferation can account for the carcinogenicity of nongenotoxic compounds. The carcinogenic dose-response relationship for genotoxic chemicals (such as 2-acetylaminofluorene) was also due in part to increased cell proliferation. Mechanistic information is required for determination of the existence of a threshold for the proliferative (and carcinogenic) response of nongenotoxic chemicals and the estimation of risk for human exposure.

CERTAIN CHEMICALS HAVE LONG BEEN ASSOCIATED WITH cancer in humans, and animal models have been developed to study processes involved in the transition from a normal to a cancer cell (1). During the past two decades, emphasis has been shifting from the use of animal models primarily for the study of carcinogenic mechanisms to the use of animals to assay for carcinogenic potential of chemicals (2). Research has been directed more at quantitatively estimating the risk to humans. Traditionally, risk assessments have entailed the use of various mathematical and statistical formulations to extrapolate from results of high-dose animal bioassays to estimates of risk at low doses (3). However, high-dose tumor response data are inadequate for this purpose, as is most evident when efforts are made to predict a threshold below which there is no effect. These limitations indicate the need to base risk assessments on knowledge of the biology of tumor formation.

S. M. Cohen is the Havlik-Wall Professor of Oncology, Department of Pathology and Microbiology, and Eppley Institute in Cancer Research, and L. B. Ellwein is Professor, Department of Pathology and Microbiology, and Associate Dean, College of Medicine, University of Nebraska Medical Center, Omaha, NE 68198.

We have developed a model of carcinogenesis, based on biological data and principles, that we originally used as an analytical tool to interpret results of experiments with the bladder carcinogen *N*-[4-(5-nitro-2-furyl)-2-thiazolyl]formamide (FANFT) in rats (4). We demonstrated quantitatively that the tumorigenic effects of FANFT administration result from its dose-dependent genotoxic and proliferative effects, and that the proliferative effects operated only at the highest doses employed (4, 5).

The model can be viewed as an assembly of dynamic relationships between variables that contribute to tumor production (Fig. 1), and incorporates several biological suppositions. A fundamental assumption is that cells exist within one of three states, normal, initiated (intermediate), or transformed, and that transitions between states occur or are irreversibly fixed only in replicating cells. These transitions are assumed to take place in a stochastic fashion and represent genetic changes introduced during cell replication, possibly with the involvement of oncogenes or tumor suppressor genes (6). Transformed cells are those that are malignant, not cells in benign lesions. In the absence of a genotoxic exposure, the probability of a transition occurring is small but not zero (thus accounting for spontaneous tumors). The likelihood of producing a cancerous cell is increased if either the probability of a genetic transition or the rate of cell replication is increased.

Another model that also incorporates the effect of cell proliferation and was validated using human epidemiology data lends further support for a two-event hypothesis for carcinogenesis (7). Although based on similar biological parameters, our model uses a different mathematical construct. To represent the biological dynamics within the target organ, we resorted to a recursive simulation. Beginning with its early development period, the status of the cell population in the target organ was computed in simulated time using the probabilities for each possible event (mitosis, genetic transition, or death) facing each cell within each of a series of specific time intervals. Calculations for each subsequent time interval incorporate the results of the preceding interval. The probabilities of mitosis or death are estimated by observation of cell proliferation and cell number at various times, and the probabilities of genetic transition were inferred by a comparison of model outcomes with